Lasers in Manufacturing Conference 2021

Monitoring of Laser Welding and Cladding Processes with Edge Artificial Intelligence Combining Thermal and Visual Cameras

Beñat Arejita[a,b,*], Juan Fernando Isaza[a], Aitzol Zuloaga[b]

[a]*EXOM Engineering, Avenida Altos Hornos de Vizcaya 33, Barakaldo, 48901, Spain*
[b]*UPV/EHU, Ingeniero Torres Quevedo Plaza 1, Bilbao, 48013, Spain*

Abstract

Laser welding and cladding are well known for their complexity and high dynamics, therefore being challenging for in situ and real-time quality control and monitoring. To tackle this challenge, this work presents a dedicated hardware implementation performing real time image processing of a multi camera configuration with a visual and a NIR camera coaxially set up with the laser beam and an off-axis stereoscopic camera. The coaxial images are analysed by edge artificial intelligence technics allowing real-time closed loop temperature control and an adaptive scanner head positioning to perform a precise melt pool monitoring and process traceability. In parallel, the volumetric positioning of the scanner head and laser job interpretation are done using the stereoscopic information, linking it with the job definition of the part being processed. The presented system can be used during Nickel-strip welding of big battery packs or during identification of milled recesses in cladding applications.

Keywords: Welding; EdgeAI; Process Monitoring; Temperature Control

1. Introduction

Laser-based manufacturing processes have been gradually introduced in the industry as the maturity of the technology has allowed tackling different industrial processes that were previously done using more traditional methods. This evolution has mainly been confirmed in laser welding, as new application areas have emerged in the last decade, such as laser battery pack welding, due to the increase in popularity of electric vehicles, and critical technology reviews such as in Zwicker et al., 2020, show the effectiveness and reliability

* Beñat Arejita. Tel.: +34 623-108-883
E-mail address: benat.arejita@exomengineering.com.

of laser welding for specific battery pack configuration and technologies. In addition to this, novel manufacturing methods for Additive Manufacturing (AM) such as Cladding or Laser Metal Deposition (LMD) have benefitted from the improvements in laser technology, optics, and digitalization, resulting in complex applications and an increase in different research works. As the manufacturing processes raise their complexity, the underlying industrial processes must provide a high degree of reliability, repeatability, and flexibility to ensure the quality of the manufactured parts, especially for short runs and on-demand production. Consequently, quality assessment methods for laser-based manufacturing processes have experienced a significant focus in the research community advancing the state of the art of quality assessment technics for complex applications such as laser welding, as shown in the review done by Stavridis et al., 2017, or other research on height control for LMD processes, Garmendia et al., 2018.

Quality assurance can be provided by passive methods that monitor the process with a range of sensors allowing both in-situ and post-process analysis and assessment of the manufactured part. Moreover, simulation techniques and digital twin models can help to improve the process by reproducing and analyzing past errors based on collected real-world process data. The reproduction of process conditions in a simulated environment and the digitization of processes have allowed the introduction of these techniques in industrial environments, Wang et al., 2020, to improve the quality of manufacturing processes and productivity. However, active techniques that adaptively control the system reacting to potential process variable modifications, such as defects in the material's microstructure, contamination on the manufacturing part surface, or uncontrolled modifications of the laser beam properties, can also significantly contribute to the final result. In the case of LMD in-process closed-loop height control, Garmendia et al., 2019, presented a method to actively control and adapt material addition in real-time, adapting the process to variations in height using a technique based on a structured light scanner. Laser-based machine vision systems have also been developed to acquire a precise geometric profile of the manufactured part combining a laser generator and a CCD camera that analyses the deformation of the laser due to the profile of the part, modifying process parameters such as the multi-axis motion system, Huang and Kovacevic, 2012. Other solutions heavily rely on image processing of the signals acquired by CCD cameras and infrared (IR) cameras. Gao et al., 2012, presented a solution based on obtaining the contour of the images of a near IR camera and calculating the gradient values of those points to detect weld deviations automatically. Automated spatter analysis has also been developed with a machine vision approach. Schweier et al., 2016, presented a method for automated spatter tracking in laser welding applications using a high-speed monochrome CMOS camera and performing an ex-post analysis of the images. As laser machine setups and processes increase their complexities, novel calibration methods may be required to use industrial imaging as part of the solution. For example, Braunreuther et al., 2015, presented a mosaicking method to detect welding joints using a CCD camera coaxially setup with a scanning optics configuration and its calibration method, illustrating the importance of operations such as the distortion correction, perspective transformation, translation and rotation correction or coordinate transformations among others, which must be applied in real-time.

The increase of computing power of small processing units, the degree of maturity of machine learning algorithms, and the digitization of the manufacturing environment drive the introduction of machine learning and artificial intelligence techniques in industrial environments with the help of edge computing devices, Carvalho et al., 2019. This allows processing data closer to the source to give a faster response to in-process real-time needs. Consequently, classic control and monitoring methods have been migrating to different machine learning techniques by the research community applying them to different laser processes. For example, Masinelli et al., 2020, presented the effectiveness of different machine learning techniques applied to acoustic signals to study both the final quality of SLM and Laser Welded parts and potential in process events that can lead to the formation of defects. On the other hand, Deep Learning (DL)techniques and especially Convolutional Neural Networks (CNN), are used to analyze images and detect or extract features for quality assurance and process monitoring purposes or as inputs to control algorithms (Bozic et al., 2020). In Contrast, Reinforcement Learning (RL) algorithms have proven to be good candidates to replace classic control algorithms, Günter et al., 2014. Additionally, machine learning techniques can also help find the most relevant factors that define or help assess laser processes, reducing the information needed to perform the quality assurance (Knaak et al., 2018).

This paper presents a versatile laser process development setup, that can be used in different implementations and research activities to introduce machine learning and AI algorithms in laser welding and additive manufacturing processes. Even though this work focuses on a laser welding use case, the system can be adapted to other processes. The paper is organized as follows: Section 2 presents the laser process development setup, describing the system as a whole and then analyzing the hardware and software elements. Section 3 presents a simple battery pack laser welding application to illustrate the proposed setup. Then, in section 4, the obtained results and a discussion are presented, and finally, in section 5, a conclusion is given.

2. Laser Process Development Setup

The primary purpose of the presented system is to provide a testbed for different laser manufacturing processes, heavily focusing on machine vision and artificial intelligence algorithms and their implementation in embedded computing devices for quality assurance and process control implementations. The following sections present the proposed system elements and their main hardware (HW) and software (SW) components.

2.1. Overall system description

As it can be seen in Fig.1, the system is composed of six main components. The scanner head has been designed to be coupled with fiber lasers up to 6000 Watts using a standard QBH connector and motorized collimator optics coupled to the laser beam input (Fig.1-a). The laser beam then passes through a beam deflection unit directing the laser radiation to different positions in the projected X-Y plane using a mounted scanning optics system (Fig.1-b). Before leaving the scanner head, the beam passes through the output optical system composed of a focusing lens, filtering optics, and a protective window (Fig.1-f). In the case of using the scanner head for cladding applications, cladding nozzles can be coupled to the scanner's output, fixing the deflection unit to direct the laser beam through the center of the cladding nozzle. Alternatively, the deflection unit can be replaced by fixed optics for cladding processes.

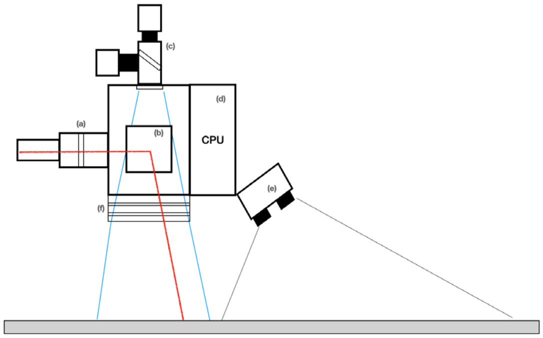

Fig. 1. High Power laser set process development setup: (a) Laser input and motorized collimator, (b) laser beam deflection unit, (c) Coaxial setup of NIR and visual camera, (d) integrated processing unit, (e) stereo camera module and (f) focusing, filtering and protective optics.

To monitor the laser process and extract meaningful information for in process quality assurance and real-time closed-loop process control, the head mounts a coaxial monitoring system that combines a visual and Near Infrared (NIR) camera using a dichroic mirror that splits the corresponding radiation bandwidth to each sensor (Fig.1-c). An optical filtering element protects both imaging sensors from laser reflections, avoiding potential permanent damages to the cameras. An off-axis machine vision module is also mounted for the pre-process analysis (Fig.1-e), combining a stereo vision camera with a high-resolution RGB camera and an embedded processing unit providing spatial AI results. The position and orientation of the off-axis machine vision module can be modified to cover different areas of interest and adapt the system to the process. Finally, the system is completed with an integrated processing unit that combines power efficient ARM cores with an embedded GPU to accelerate machine learning and AI algorithms and a Field Programable Gate Array (FPGA) performing real-time control tasks (Fig.1-d). The modular design is intended to provide a high degree of adaptability and customization to allow using the setup in different laser processes.

2.2. HW and SW design

The process control and monitoring unit is an embedded heterogeneous multiprocessing system that combines a Xilinx Ultrascale+ ZU3EG MPSoC (FPGA+ARM) with an Nvidia Jetson Nano (GPU+ARM) and an OpenCV AI Kit (OAK-D) with a Video Processing Unit (VPU) capable of running spatial AI algorithms depicted in Fig.2. While the OAK-D is used for pre-process monitoring and control tasks, the combined Jetson Nano and the MPSoC are used for in-process tasks using the images acquired from the visual and NIR cameras coaxial setup. The OAK-D combines an Intel Movidius Myriad X processor with a stereo camera with two global shutter OV9282 sensors (1280x800 max 120fps) and a high-resolution IMX378 sensor (4056x3040 max 60 fps) with autofocus. The openVINO framework is used to optimize pre-trained deep learning models for the Myriad X processor, and inferencing, detection, or segmentation algorithms can efficiently be run at 30 fps in the camera module. Using the Depthai API, spatial AI algorithms can be run aggregating spatial information to the deep learning models. The OAK-D is mounted off-axis in the scanner head and runs the software for pre-process analysis, aiding the scanner head positioning system by providing spatial information over CANopen to the machine. For in-process image processing tasks, the Nvidia Jetson Nano is used, taking advantage of its Maxwell architecture GPU with 128 CUDA cores. Using the JetPack framework then allows building AI applications that are optimized to run in the CUDA cores, accelerating machine learning and deep learning algorithms in the GPU. The Jetson Nano is connected to a global shutter Vision components MIPI IMX296-C camera module with a resolution of 1440x1080 at 60 fps for the image acquisition.

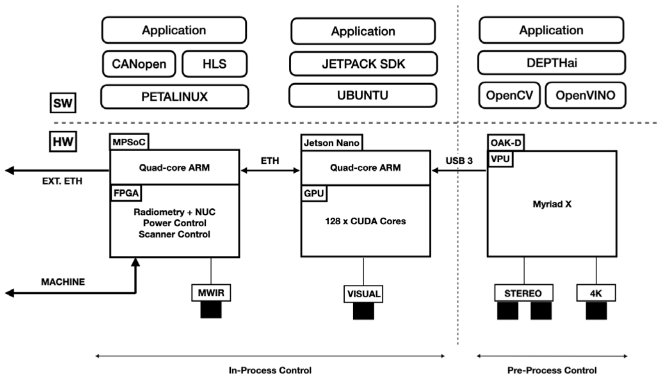

Fig. 2. Process Control and monitoring general HW and SW diagram.

The real-time process control tasks are done in the MPSoC to assure that all the timing constraints are met, and a hard real-time behavior is provided. The laser beam scanning control, the infrared image nonuniformity correction, the radiometric calibration, and the IR image-based closed-loop laser power control are done in the FPGA. On the other hand, the high-level scanning and power strategies are selected and commanded by the embedded Linux that runs on the ARM processor using the computed information from the on-axis and off-axis camera systems coming from the Jetson Nano and the OAK-D. A NIT Tachyon 1024 microCAMERA is used for the infrared image acquisition, providing images in the MWIR band with a sensor resolution of 32x32 and a framerate of 1000 fps.

3. Use case: Simple battery pack classification and welding

3.1. Use case description and application design

A simple use case has been designed to validate the proposed architecture. The use case consists of detecting a set of simple battery packs for the precise welding of the battery cells to the connection strips. For that purpose, the off-axis camera module is configured to detect and provide spatial information of the battery as the laser head approaches to aid in its positioning. Once the scanner head is correctly positioned, the on-axis visual system detects the battery pack to select the proper welding strategy from a set of stored welding strategies and provide a bounding box to the battery cell connection detector. The welding strategy depends on the battery pack type and the battery cell connection (positive or negative), modifying the scanning strategy and the power control profile. Some welding strategy results can be seen in Appendix A. To precisely track the connector positions, the acquired images are first transformed into HSV images and thresholded, getting a binary image. The binary image is then dilated to detect the cell connections and the center coordinates more precisely. As the connections are tracked, the detected coordinates are sent to the scanner controller to apply real-time corrections. In parallel, the same information is sent to the power control and temperature monitoring module to apply the correct area of interest while welding. The temperature is constantly monitored to avoid potential battery cell damages, adapting the power to match the most suitable temperature profile, or disable the laser if necessary.

3.2. System calibration

3.2.1. IR camera: Non-Uniformity Correction and Radiometric calibration

The Tachyon 1024 microCAMERA provides raw images with 10 bits of resolution per pixel. The pixel value depends on the radiation flux that reaches the sensor, but due to tolerances in the sensor manufacturing process, each pixel reacts differently to the same amount of radiation, causing a non-uniformity in the image. To correct this effect, we have implemented the algorithm presented by Orzanowski, 2016, directly in the FPGA, and the images are corrected as they enter the processing pipeline. Equation 1 shows the transformation operation from raw pixel values $x_i(\phi)$ to converted pixel values $y_i(\phi)$.

$$y_i(\phi) = [x_i(\phi) - s_i(\phi)]g_i + o_i + s(\phi) \tag{1}$$

$$g_i = \frac{\Delta x(\phi)}{\Delta x_i(\phi)} = \frac{x(\phi_2) - x(\phi_1)}{x_i(\phi_2) - x_i(\phi_1)} \quad , \quad o_i = [s_i(\phi_r) - x_i(\phi_1)]g_i + x(\phi_1) - s(\phi_r)$$

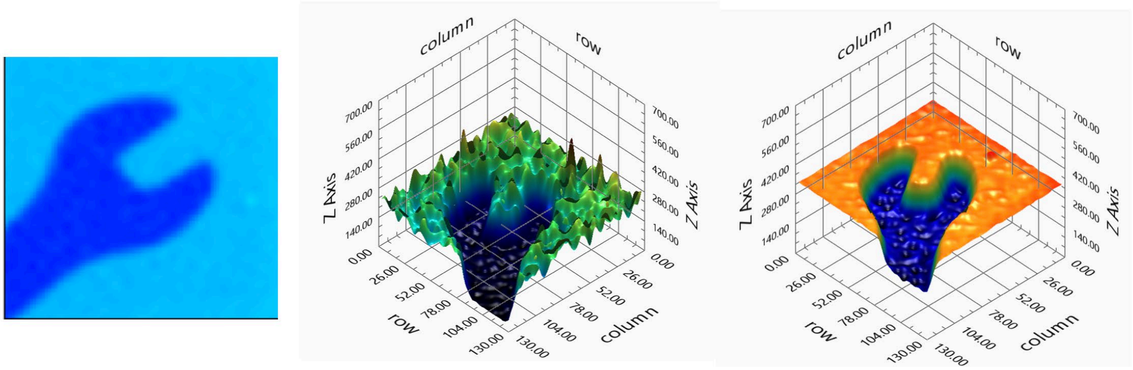

(a) (b) (c)

Fig. 3. IR camera non-uniformity correction and radiometric calibration results (interpolated to 128x128): (a) 8 mm wrench between the calibration blackbody radiator and the camera, (b) Tachyon 1024 microCAMERA raw values without non-uniformity correction and radiometric calibration (z axis - sensor pixel counts), (c) corrected IR image with non-uniformity correction and radiometric calibration (z axis - temperature in degrees Celsius)

Where $x_i(\phi_1)$ and $x_i(\phi_2)$ are the time averaged i-th pixel value at high and low reference temperatures, $x(\phi_1)$ and $x(\phi_2)$ are the frame averages at high and low temperatures, and $s_i(\phi_r)$ and $s(\phi_r)$ are the time average of the i-th pixel and the frame average when the shutter is closed at a sensor reference temperature.

Additionally, a radiometric calibration must be performed to convert IR sensor pixel values to temperature. One of the most common functions to convert the sensor signal into temperature is the Sakuma-Hattori equation, an approximation to the Planck's radiation equation (Olsen et al., 2018). Equation 2 shows the inverse Sakuma-Hattori equation, which has also been implemented in the FPGA after the non-uniformity correction is done, providing the apparent black body radiator temperature. The temperature of the object is then obtained by applying the emissivity factor of the material.

$$F^{-1}(S) = T_{app} = \frac{c_2}{A\ln\left(C/S+1\right)} - \frac{B}{A} \qquad (2)$$

Where c_2 is the second radiation constant ($0.014387752\ m \cdot K$), A, B and C are the regression constants, S the sensor value and T_{app} is the apparent black body radiator temperature. The non-uniformity correction and the radiometric calibration have been done with an Optris BR400 blackbody radiator for the ranges between 200 and 400 degrees Celsius, obtaining an accuracy of +/- 5 °C. Fig.3 shows the differences before and after applying the non-uniformity correction and the radiometric calibration when the path between the IR camera and the black body, set to 320 °C, is blocked using an 8 mm wrench.

3.2.2. Image space coordinate transformation

The on-axis system comprises three elements: the laser scanner, the coaxial visual camera, and the coaxial IR camera, each with their respective coordinate system. To relate the coordinate systems between all three image spaces, a coordinate calibration must be done. A transformation function from image space coordinates to real-world coordinates can be computed using a chessboard with known square sizes. We have used affine transformation matrices for the coordinate transformation function in this work as all three image projections share the same plane. The affine transformation is a well-known transformation that can be expressed with the algebraic equations in Equation 3 (Bebis et al., 1999).

$$T = A \cdot \begin{bmatrix} x \\ y \end{bmatrix} + B \quad , \quad A = \begin{bmatrix} a_{00} & a_{01} \\ a_{10} & a_{11} \end{bmatrix}_{2\times 2} B = \begin{bmatrix} b_{00} \\ b_{10} \end{bmatrix}_{2\times 1} \tag{3}$$

In order to resolve each affine transformation matrix, three different point pairs must be collected. Each point pair comprises an x,y coordinate in the image space (pixels or scanner steps) and the same point in real-world coordinates. In the case of the IR camera, an infrared emitter has been used to identify the pixels of interest in the IR image space. Once all three affine transformation matrices are calculated, it is possible to transform the coordinates from one image space to another.

3.3. Battery Pack detection model

We have selected Mobilenet-SSDv2 to detect the different battery packs of the use case. Mobilenet-SSDv2 has been designed to efficiently classify and position objects, making it suitable for embedded platforms with memory and processing limitations (Chiu et al., 2020). The training started from a pre-trained model, and then we applied transfer learning to tune it to detect the battery packs. The same model is used in the Jetson Nano and the OAK-D, while the model in the Jetson Nano is used to detect the pack and select the corresponding welding strategy once the scanner head has been positioned, the model in the OAK-D is used to detect the battery pack and get its spatial information for positioning purposes in the pre-processing phase. The model for the OAK-D was additionally optimized for the myriad X processor using the openVINO framework.

A dataset of 1000 images for each type of battery pack was collected in the VOC format to train the detection model. The images were taken using different perspectives, lighting conditions, and battery pack orientations. Once the dataset was collected and properly tagged, it was divided into three different image sets: training, validation, and testing. While the training data set is used to fix the model parameters, the validation data set is used to evaluate them as the training goes on, and finally, the test data set provides an evaluation of the final model. 70% of the dataset images were used for training, 20% for validation, and 10% for testing. The obtained training and validation loss values is shown in Fig.4.

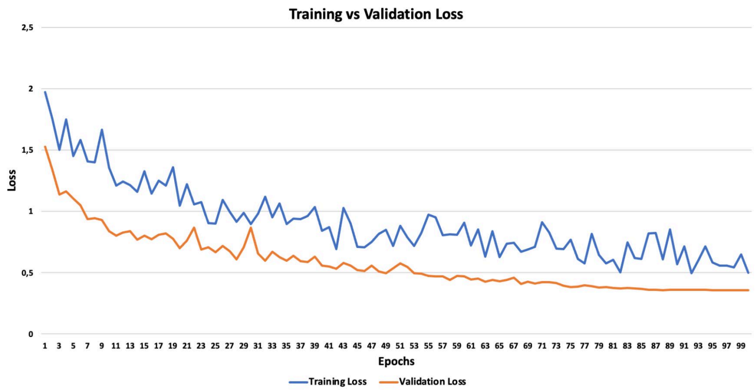

Fig. 4. Mobilenet-SSDv2 model retraining vs validation loss graph.

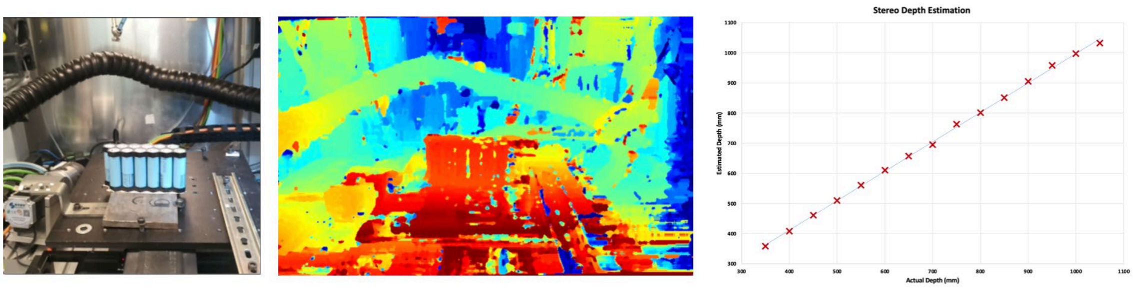

(a) (b) (c)

Fig. 5. Pre-process monitoring system results: (a) RGB image obtained from the OAK-D targeting a type b battery pack in the laboratory setup, (b) Depth map of the detected battery pack provided by the stereo system of the OAK-D, (c) Stereo depth estimation vs actual depth.

4. Results and Discussion

4.1 Pre-Process Monitoring

The battery pack detection model was uploaded to the OAK-D so that the scanner head could scan the front area, acquire volumetric information of the surroundings, and detect the battery packs providing their spatial information in millimeters. Due to the limitations of the stereo camera, the detection range was set between 300 and 1100 mm. Fig.5. shows some of the results we obtained in the tests. While the acquired depth map captured the battery pack correctly in the test setup, it must be noted that objects with high reflectivity were difficult to detect. Fig.5-a and Fig.5-b show the difference between the acquired visual images and the corresponding depth map. The depth information was tested positioning the stereo camera to different distances from the battery pack, and the obtained results are shown in Fig.5-c. On average, the estimated depth's accuracy was +/- 10 mm for the range under test. Nevertheless, as the battery pack was approached to the measuring lower limit, the measurements tended to be more unstable, as the disparity map presented significant errors. Additional depth map post-processing could significantly help to stabilize the measurements. Additionally, illumination plays an essential role in the accuracy of the depth estimation. As in low light situations, the spatial information is not very reliable active lighting strategies can help improve object detection and spatial information estimation.

4.2 In-Process Monitoring

The trained model successfully detected the battery packs' position with accuracy, setting the bounding box for the cell connection detection algorithm. In addition to this, the confidence level of the battery pack classification was greater than 98% (Fig.6-a), and it was able to differentiate between the trained battery packs. Nevertheless, it detects some objects as battery types generating a false positive, suggesting that the model should be re-trained, including other types of objects in the dataset. The connection detection algorithm received as input the bounding box of the detected battery pack and successfully detected connectors after the corresponding HSV image thresholding and dilating the resulting image (Fig.6-b). Then, the connection detector extracted the connector's center coordinate to transmit it to the laser beam scanning controller to adapt the welding strategy dynamically (Fig6-c) with an accuracy of +/- 1 mm. In parallel, the IR image monitor also uses the connection center point coordinates to monitor the temperature levels of the connection and assure that the temperature never reaches levels that could damage the battery cell. As with the depth detector, the connector detector showed the importance of the illumination and the need to adaptively controlling it to assure optimal machine vision conditions.

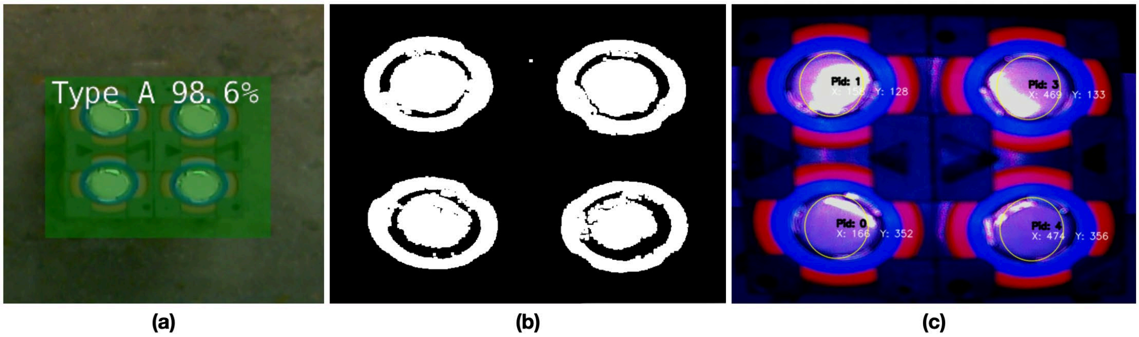

Fig. 6. Battery pack type detection and connector identification: (a) Type A battery pack is detected with a confidence level greater than 98%, (b) Threshholded and dilated top view image of the battery pack for connection coordinate detection, (c) Detection of connections to be welded to a connection bar and their center coordinates.

5. Conclusions and future work

In this work, we have presented a versatile laser process development setup to be used as a platform to integrate and research machine vision and artificial intelligence algorithms and their application to laser manufacturing processes, emphasizing their implementation in constrained embedded processing units. A simple use case covering all the setup elements, which consisted of detecting the contact points in a simple battery pack welding application, was introduced to validate and test the proposed system. The Mobilenet-SSDv2 model was successfully retrained to detect the battery packs of the use case, which was used in both the on-axis and off-axis camera settings. While the off-axis camera module successfully provided the depth map of the surroundings and detected battery packs and their spatial information, the on-axis camera setup detected the battery cell connectors providing the coordinates for the scanner controller and the closed-loop power control module. The results validated the proposed architecture as a suitable platform to test the application of edge artificial intelligence in laser manufacturing processes. Future work will address the development of artificial intelligence algorithms to tackle specific problems in laser manufacturing, with a particular focus on laser welding and laser cladding applications, where in addition to deep learning techniques for object classification and detection, decision-making algorithms, and reinforcement learning applied to control tasks will be deeply studied.

Acknowledgements

The work presented in this paper is under the framework of the Neotec Project SOLAMARE. This project has received funding from the Spanish Ministry of Science and Innovation through the Centre for the Development of Industrial Technology (CDTI) under agreement No. SNEO- 20191298. The dissemination of results herein reflects only the authors' view, and the CDTI is not responsible for any use that may be made of the information it contains. We would also like to thank Alterity for their support and provisioning of battery cells, and battery packs for the laser welding tests carried out.

References

Zwicker, M. F. R., Moghadan M., Zhang W., Nielsen C. V., 2020. "Automotive battery pack manufacturing - a review of battery to tab joining", Journal of Advanced Joining Processes, vol. 1.

Stavridis, J., Papacharalampopoulos, A. & Stavropoulos, P, 2018. "Quality assessment in laser welding: a critical review", Int J Adv Manuf Technol, Issue 94, p.1825.

Garmendia, I., Leunda, J., Pujana, J., Lamikiz, A., 2018. "In-process height control during laser metal deposition based on structured light 3D scanning". Procedia CIRP 68, p. 375.

Wang, B., Hu, S. J., Sun, L., Freiheit, T, 2020. "Intelligent welding system technologies: State-of-the-art review and perspectives", Journal of Manufacturing Systems 56, p. 373 .

Garmendia, I., Pujana, J., Lamikiz, A., Madarieta, M., Leunda, J, 2019. "Structured light-based height control for laser metal deposition", Journal of Manufacturing Processes 42, p. 20.

Huang, W., Kovacevic, R, 2012. "Development of a real-time laser-based machine vision system to monitor and control welding processes", Int J Adv Manuf Technol 63, p. 235.

Gao, X., You, D., Katayama, S, 2012. "Infrared image recognition for seam tracking monitoring during fiber laser welding", Mechatronics 22, p. 370.

Schweier, M., Haubold, M. W., Zaeh, M. F, 2016. "Analysis of spatters in laser welding with beam oscillation: A machine vision approach", CIRP Journal of Manufacturing Science and Technology 14, p. 35.

Braunreuther, S., Hammerstingl, V., Schweier, M., Theodossiadis, G., Reinhart, G., Zaeh, M.F., 2015. "Welding joint detection by calibrated mosaicking with laser scanner systems", CIRP Journal of Manufacturing Science and Technology 10, p. 16.

Carvalho, A., Mahony, N. O., Krpalkova, L., Campbell, S., Walsh, J., Doody, P., 2019. "Edge Computing Applied to Industrial Machines", Procedia Manufacturing 38, p. 178.

Masinelli, G., Shevchik, S.A., Pandiyan, V., Quang-Le, T., Wasmer, K., 2021. "Artificial Intelligence for Monitoring and Control of Metal Additive Manufacturing", in Meboldt M., Klahn C. (eds) Industrializing Additive Manufacturing. Springer, p. 205.

Božič, A., Kos, M., Jezeršek, M, 2020. "Power Control during Remote Laser Welding Using a Convolutional Neural Network", Sensors 20, 6658.

Günther, J., Pilarski, P. M., Helfrich, G., Shen, H., Diepold, K., 2014. "First Steps Towards an Intelligent Laser Welding Architecture Using Deep Neural Networks and Reinforcement Learning", Procedia Technology, vol. 15, p. 474.

Knaak, C., Thombansen, U., Abels, P., Kröger, M, 2018. "Machine learning as a comparative tool to determine the relevance of signal features in laser welding", in Procedia CIRP, vol. 74, p. 623.

Orżanowski, T., 2016. "Nonuniformity correction algorithm with efficient pixel offset estimation for infrared focal plane arrays", SpringerPlus 5, 1831.

Olsen, Å. A. F., Mathisen, H., Simonsen, S, 2018. "An investigation into a calibration scheme for a light pipe based temperature probe", Meas. Sci. Technol. 29, 115004.

Bebis, G., Georgiopoulos, M., Lobo, N. V., Shah, M., 1999. "Learning affne transformations", Pattern Recognition, vol. 32, i. 10, p. 1783.

Chiu, Y.-C., Tsai, C.-Y., Ruan, M.-D., Shen, G.-Y., Lee, T.-T, 2020. "Mobilenet-SSDv2: An Improved Object Detection Model for Embedded Systems", in 2020 International Conference on System Science and Engineering (ICSSE), p. 1 .

Appendix A. Welding strategy examples

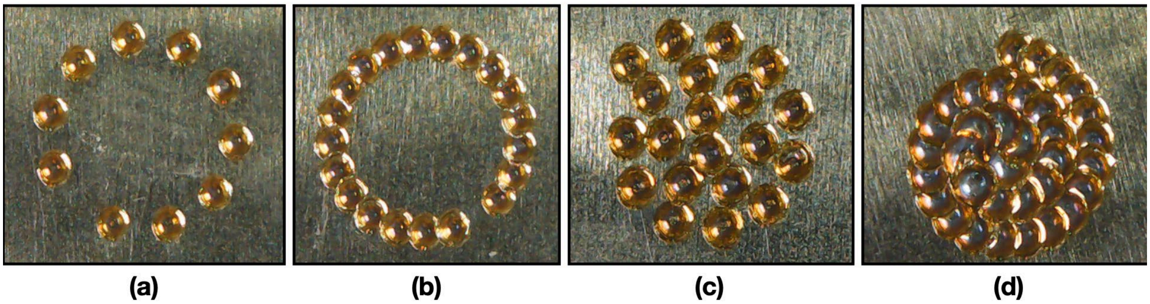

Fig. 7. Different welding strategy results using a pulsed laser and output power of 2 kW: (a) 4 mm width circle with 10 pulses, (b) 4 mm width circle with 20 pulses, (c) 4 mm width spiral with 20 pulses, (d) 4 mm width spiral with 40 pulses.